# Modeling of the HCPB Helium Coolant Purification System for EU-DEMO: Process Simulations of Molecular Sieves and NEG Sorbents

Jonas C. Schwenzer, Alessia Santucci & Christian Day

# Modeling of the HCPB Helium Coolant Purification System for EU-DEMO: Process Simulations of Molecular Sieves and NEG Sorbents

Jonas C. Schwenzer,[a]* Alessia Santucci,[b] and Christian Day[a]

[a]*Karlsruhe Institute of Technology, Institute for Technical Physics, Eggenstein Leopoldshafen, Germany*
[b]*ENEA, Fusion and Technology for Nuclear Safety and Security Department, Rome, Italy*

**Abstract** — *The Helium Cooled Pebble Bed breeding blanket of the EU-DEMO foresees continuous processing of a small fraction of the helium coolant in the coolant purification system (CPS) to counteract buildup of tritium and impurities. For this system, two different process variants are currently considered. The first is based on the conversion of all hydrogen species into water using copper oxide beds and the subsequent water adsorption over zeolite molecular sieve (ZMS) beds. The alternative process foresees the direct sorption of hydrogens onto novel ZAO® non-evaporable getter (NEG) materials. The ZMS beds and the NEG beds are operated batchwise, but alternating schemes with an absorption (operation) phase and a desorption (regeneration) phase result in a pseudocontinuous process. Transient process simulations have been developed to evaluate the performance and impact of the different variants on downstream systems in the fuel cycle. In this contribution, these process models for the preconceptual design of both variants are presented and evaluated. For the reference designs proposed for each system, they have been found to satisfy the requirements of achieving 90% efficiency. This modeling then lays the foundation for optimization of the conventional process and outlines further research demand regarding the application of NEG materials needed to progress toward the concept design of the CPS process.*

**Keywords** — *Fuel cycle, coolant purification, process modeling.*

## I. INTRODUCTION

One of the two breeding blanket concepts currently under investigation in the EU-DEMO program is the Helium Cooled Pebble Bed (HCPB) breeding blanket. The blanket is cooled with helium at $p = 8$ MPa and up to $T = 793.15$ K (Ref. 1). Because of the high temperatures and close proximity of tritium in the breeding sections of the blanket, tritium can permeate into the coolant and has to be removed therefrom to combat further propagation through the power cycle.[1,2] For this reason, a coolant purification system (CPS) is employed with the aim of removing the permeated tritium and limiting the partial pressure of HT in the coolant to a level below $4 \times 10^{-2}$ Pa (Ref. 1). As further measures to limit tritium permeation into the coolant, the addition of protium at levels of 80, 300, or 1000 Pa is under consideration,[3] which then also constitutes an additional load for the system.

The preconceptual design phase of the EU-DEMO has identified two technology variants for the CPS (Ref. 4). The first is based on the ITER Test Blanket Module (TBM) CPS, utilizing copper oxide conversion beds and zeolite molecular sieves (ZMSs) (referred to as ZMS variant in the following).[5] The second process variant uses non-evaporable getter (NEG) materials for the direct absorption of hydrogen (NEG variant).[3] Figure 1 shows the process layout for both variants taken as

*E-mail: jonas.caspar.schwenzer@kit.edu

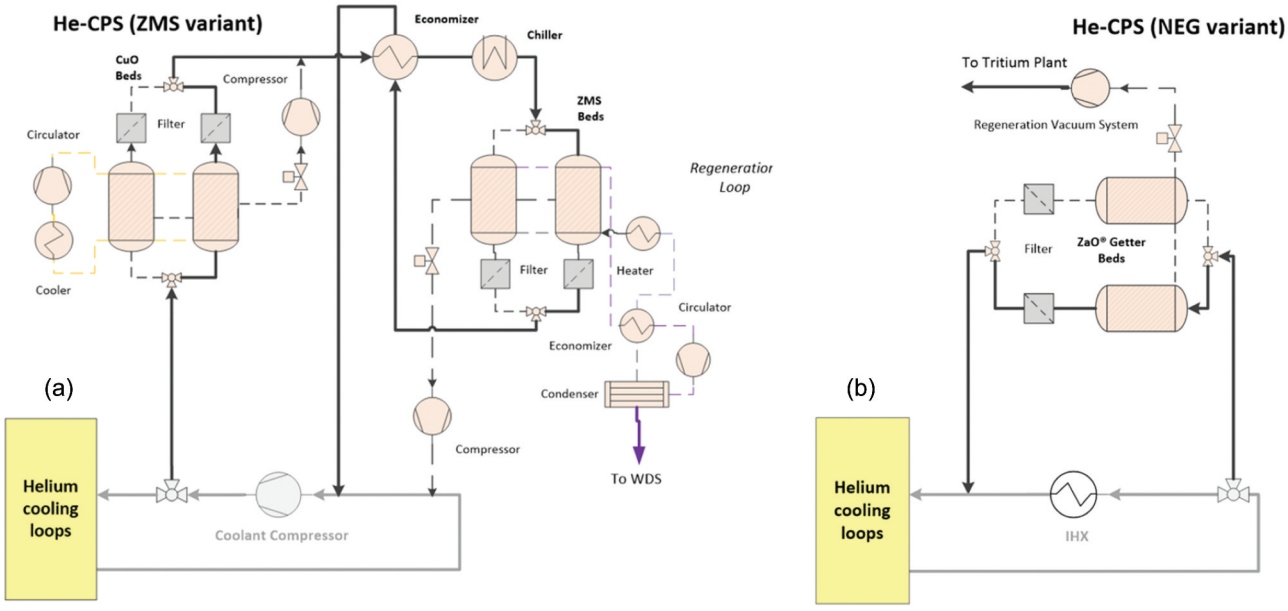


Fig. 1. Layout of the two technology variants for the helium CPS in the EU-DEMO fuel cycle. The left process variant (a) is based on the ITER TBM CPS process and uses copper oxide beds to convert hydrogen contained in the coolant into water and adsorb it on ZMS beds. The right process variant (b) relies on the direct absorption of hydrogen on NEG beds.

a basis for the process simulation, with the requirements and dimensioning of the systems investigated based on the preconceptual design status thereof described in Refs. 1, 3, and 4.

In the ZMS process, a fraction of the coolant stream is extracted after the main coolant compressor and routed over a copper oxide bed, converting the contained hydrogen into water. The stream is then cooled down and passed over a bed of ZMS 4A, where the formed water is adsorbed. The outgoing stream is used to precool the incoming stream in an economizer and then is reintroduced into the coolant upstream of the compressor, using the pressure differential to drive the process. Once saturated, the molecular sieve bed is regenerated by decoupling it from the process, depressurizing to ambient level, and purging it with hot inert gas in counterflow direction. The purge gas is hereby circulated in a closed loop, and a condenser is used to remove the desorbed water.

In the NEG process variant, a fraction of the coolant is extracted on the high-temperature side before the primary heat exchanger [intermediate heat exchanger (IHX)], routed directly over a getter bed of ZAO® (Zr-V-Ti-Al) (Ref. 6) alloy and then introduced back into the coolant after the IHX. Once a bed is saturated, it is decoupled, depressurized, and evacuated to regenerate the getter. For the purpose of this study, it is assumed that the regeneration that occurs isothermal, as no heated fluid can be circulated through the bed and no design using internal heating is currently available. This has the additional benefit of avoiding thermal cycling stress of the structural material operating at the already strenuous conditions of the coolant loop hot leg. Furthermore, the application of this getter material is restricted to process conditions where the resulting hydrogen loading does not exceed 13 $Pa \cdot m^3 \cdot g^{-1}$ (Ref. 7), as too high hydrogen concentrations lead to embrittlement in the material, making it unfavorable for long-term application as foreseen here.

Because of their semicontinuous nature of loading and regeneration cycles, both process variants require the use of two or more beds in parallel to enable continuous processing of the coolant. This further requires that regeneration be achieved faster than the loading phase (with cycle time $\tau_c$). As DEMO utilizes a closed fuel cycle, the streams discharged from the system in the regeneration phase are further processed to make the contained tritium available for fueling.

Process modeling and simulation are valuable tools for the process designers to make predictions of the achievable efficiency of the process, the amount of sorbents required to achieve a desired cycle time, and the characteristics of the systems' exhaust stream sent for further processing. This paper presents the simulation developed for the two outlined process variants. Section II gives the mathematical model of the sorption bed used. Section III then presents results for a simulation case representing the preconceptual design of both systems, and Sec. IV

discusses the consequences for the process and its integration in the fuel cycle. Section V concludes the paper.

## II. MODEL

The key component in each system is the sorption bed, and consequently, this also is the focus of the modeling. The bed is assumed as a homogeneous packed bed of uniform spherical particles of diameter $d_p$ (for both NEG[a] and ZMS variants) with fluid flow along the length axis $x$ of the bed. Assuming uniform flow characteristics across the diameter of the bed, the fluid flow along the length can be described by a molar balance around an infinitesimal volume element of the bed Eq. (1) and Ergun Eq. (2) (Ref. 8), linking the pressure drop across an element with the throughput:

$$\frac{dN_{i,f}}{dt} = \frac{V}{zRT}\left(p\frac{dy_i}{dt} + y_i\frac{dp}{dt} - \frac{y_i p}{T}\frac{dT}{dt}\right) = \frac{dF_{i,f}}{dx} - \frac{dN_{i,s}}{dt} \tag{1}$$

and

$$\frac{dp}{dx} = \frac{150\eta RT(1-\in)^2}{pd_p^2\in^3\frac{\pi}{4}d_b^2}F_f + \frac{1.75M_f RT(1-\in)}{pd_p\in^3\left(\frac{\pi}{4}d_b^2\right)^2}F_f^2\ , \tag{2}$$

where

$R$ = universal gas constant
$V$ = volume
$T$ = temperature
$p$ = pressure
$F$ = molar flow rate of fluid
$\in$ = porosity of the bed
$d$ = bed diameter
$\eta$ = fluid viscosity
$M_f$ = molar mass of the fluid, assumed to be that of pure helium
$z$ = compressibility factor, assumed constant over the range of temperature and pressure variations during a take-up or regeneration cycle.[b]

The molar balance is stated for each individual species $i$ in the fluid phase of the volume element, as well as for the overall molar holdup $N_f$, obtained when setting the sum of molar factions $y_i$ to one. The model is assumed to be quasi stationary with regard to pressure transients once the sorption phase is established so that $dp/dt = 0$.

As the NEG bed is regenerated at the same temperature as during the sorption phase, and the heat of absorption is small when compared with the total throughout, isothermal operation is assumed so that $dT/dt = 0$ for that variant. The ZMS bed is heated up for regeneration by the hot purge gas, and transient energy balances are used to describe the fluid and solid phase:

$$N_f \cdot c_{p,f} \cdot \frac{dT_f}{dt} = c_{p,f}\frac{d\left(F_f T_f\right)}{dx} - \alpha \cdot a_s V \cdot \left(T_s - T_f\right) \tag{3}$$

and

$$\left(m_s \cdot c_{p,s} + q \cdot m_s \cdot c_{p,i}\right)\frac{dT_s}{dt} = \alpha \cdot a_s \cdot \left(T_s - T_f\right) + h_{ad} \cdot \frac{dN_s}{dt}\ , \tag{4}$$

where

$c_{p,f}$ = molar heat capacity of the fluid
$a_S$ = specific surface area of the sorbents
$\alpha$ = heat transfer coefficient
$m_s$ = mass of the sorbents
$c_{p,s}$ = sorbents mass heat capacity
$q$ = loading of the sorbents ($mol \cdot kg^{-1}$)
$h_{ad}$ = heat of adsorption
$c_{p,i}$ = molar heat capacity of the sorbate.

The numeric solution of Eqs. (1) through (4) requires the specification of boundary and initial conditions (see Table I). Dirichlet (fixed) boundary conditions are used on the side where the feed stream is introduced ($x = 0$), and values are set to that of the feed stream. Neumann boundary conditions are stated at the other end ($x = l$).

[a] For comparability reasons, here we assume the shape of the NEG material to also be spherical pellets, in which they are not yet available commercially in large quantities. Since similar shapes exist (e.g., sintered disks), we think this extrapolation is permissible.

[b] Throughout this paper, units of symbols in equations are understood to be SI units or SI-derived units unless specified otherwise.

TABLE I

Boundary and Initial Conditions of the Conservation Equations Used in the Model

| Boundary Conditions | |
|---|---|
| Sorption Phase | Regeneration (ZMS only) |
| $F_i(x=0) = const. = F_{feed}$<br>$p(x=0) = const. = p_{feed}$<br>$T(x=0) = const. = T_{feed}$<br>$\frac{dp(x=l)}{dx} = \frac{dF_i(x=l)}{dx} = \frac{dT(x=l)}{dx} = 0$ | $F_i(x=l) = const. = F_{reg}$<br>$p(x=l) = const. = p_{reg}$<br>$T(x=l) = const. = T_{reg}$<br>$\frac{dp(x=0)}{dx} = \frac{dF_i(x=0)}{dx} = \frac{dT(x=0)}{dx} = 0$ |
| Initial Conditions | |
| $T(t=0,x) = T_{feed}$<br>$p(t=0,x) = p_{feed}$<br>$N_s(t=0,x) = 0$<br>$N_{fi}(t=0,x) = \frac{p_{feed,i} V_n}{zRT_{feed}}$ | |

The sorption behavior of the bed is governed by the sorption rate $\frac{dN_{i,s}}{dt}$, which is given by a first-order kinetic expression that sets the sorption rate proportional to the difference between equilibrium and current loading at the given pressure and temperature, with the proportionality constant being the mass transfer coefficient (MTC). The description of the equilibrium is unique to each system, whereas similar transport mechanisms that govern the MTC apply in both cases.

The model has been implemented in and numerically solved with the Aspen® Custom Modeler V12, using a mixed Newton nonlinear solver and implicit Euler integrator. The minimum integration time step size was selected as 0.001 s, and a convergence criterion of 1e-5 relative and absolute error was set. Following a grid independency study, a length discretization into 80 elements was found sufficient in both cases.

## II.A. NEG Sorption Equilibrium

The sorption equilibrium of diatomic gases between its partial pressure in the gas above the surface ($p_{i,surf}$ in Torr) and its concentration in the metal particle ($c_{i,part}$ in Torr·L·g$^{-1}$) can be described by Sievert's law[9] as

$$c_{i,part} = \sqrt{K_s p_{i,surf}}\ , \tag{5}$$

where $K_s = 10^{-\left(5.76-\frac{7290}{T}\right)}$ Torr·L$^2$·g$^{-2}$ (Ref. 7) for the here employed NEG material and hydrogen (using all hydrogen isotopes). Figure 2b shows the equilibrium loading as a function of hydrogen pressure and temperature. It immediately becomes obvious that operation on the high-temperature side (before the IHX) of the coolant loop is favorable for the here considered levels of hydrogen

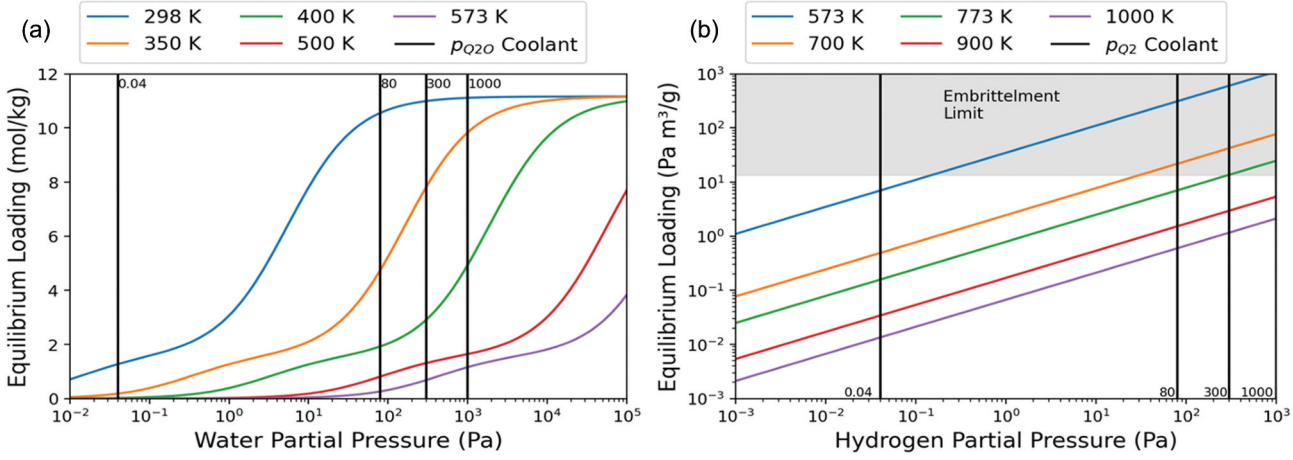


Fig. 2. Equilibrium loading relationships for (a) ZMS and (b) NEG.

partial pressure due to the high achievable loading while not encountering the embrittlement limit in cases of 80 and 300 Pa $H_2$ addition. The case of 1000 Pa $H_2$ addition is nevertheless deemed unfeasible without additional measures (higher operation temperature or artificial dilution).

## II.B. ZMS Sorption Equilibrium

For zeolites of type 4A as employed here, the equilibrium loading with adsorbed water $q^*_{Q2O}$ in mol·kg$^{-1}$ as a function of water partial pressure $p_{Q_2O}$ in bars ($Q_2O$ referring to waters independent of the involved hydrogen isotopologues) is described by a dual site Langmuir isotherm of the form

$$q^*_{Q2O} = \frac{q_\alpha b_\alpha p_{Q_2O}}{1 + b_\alpha p_{Q_2O}} + \frac{q_\beta b_\beta p_{Q_2O}}{1 + b_\beta p_{Q_2O}} , \tag{6}$$

with $b_{\alpha,\beta} = b_{\alpha,\beta,0}\exp\left(\frac{E_{\alpha,\beta}}{RT}\right)$ and parameter values as given in Table II (Ref. 10).

Figure 2a shows the equilibrium loading as a function of temperature and water partial pressures (assumed here to be that of $H_2O$ and HTO). At 298 K, all cases of protium addition allow operation near the capacity limit of $q_\alpha + q_\beta = 11.16$ mol·kg$^{-1}$.

## II.C. Mass Transport Coefficient

The uptake of the sorbate in the particle can be limited by the transport through the fluid boundary layer forming around the particle, the diffusive transport in the particle, or the surface reaction rate in the case of the NEG system.

For the here relevant range of Reynolds numbers, the boundary layer transport can be described by the Sherwood number and using the Sherwood correlation of Wakao for a packed bed[11]:

TABLE II

Parameter Values for the Dual Site Langmuir Isotherm

| | $q$ (mol·kg$^{-1}$) | $E$ (kJ·mol$^{-1}$) | $b_0$ (bar$^{-1}$) |
|---|---|---|---|
| α | 9.57 | 56.86 | 2.02e-6 |
| β | 1.59 | 53.50 | 3.24e-3 |

$$\mathrm{Sh} = \frac{k_f d_p}{D_m} = 2 + 1.1\mathrm{Sc}^{\frac{1}{3}}\mathrm{Re}^{0.6} , \tag{7}$$

where

$k_f$ = fluid side transport coefficient (m·s$^{-1}$)

$D_m$ = diffusion coefficient of species $i$ in the bulk fluid

$\mathrm{Sc} = \frac{v}{D}$, $\mathrm{Re} = \frac{ud_p}{v}$ = Schmidt number and Reynolds number, respectively, with $v$ the kinematic viscosity of the fluid and $u$ the superficial bulk fluid velocity.

### II.C.1. ZMS Variant

In the case of the ZMS beds, intraparticle transport is not negligible due to the lower temperature and the fact that transport of the larger-molecule water is slower. The total combined mass transfer coefficient is therefore given by addition of the resistances as

$$\mathrm{MTC}^{-1} = \left(\frac{d_p}{6k_f} + \frac{d_p^2}{60\in_b D_{eff}}\right)^{-1} , \tag{8}$$

with $k_f$ evaluated as above and the second term being the linear driving force coefficient as given by Glueckauf,[12] to describe the intraparticle transport. $\in_b$ is the total void fraction (dimensionless), combining the porosity of the bed and that of the ZMS particles. The effective diffusion coefficient $D_{eff}$ in the particle is given as a superposition of molecular diffusion in the macropores and Knudsen diffusion in the micropores:

$$\frac{1}{D_{eff}} = \tau\left(\frac{1}{D_k} + \frac{1}{D_m}\right)^{-1} , \tag{9}$$

where $\tau$ is the pellet tortuosity (dimensionless). For simple molecules in porous zeolites in the temperature range of interest, the Knudsen diffusion coefficient is given by $D_k = 9700 r_p\sqrt{\frac{T}{M}}$ (Ref. 13), and the molecular diffusion coefficient $D_m$ is evaluated using the Fuller equation for a binary system of carrier gas and sorbate.[14]

### II.C.2. NEG Variant

Because of the higher operating temperature of the NEG bed (resulting from the upstream positioning of IHX), intraparticle diffusion proceeds fast enough as to not be rate limiting[7] while the particle size in the packed bed is selected small enough as to prevent surface limitations. The MTC is then given as MTC $= k_f$ for the NEG variant.

Figure 3 shows an illustration of the concentration profiles of the sorbate in the fluid phase and particle. The negligible intraparticle transport resistance for the NEG leads to a uniform concentration distribution in the particle, whereas in the ZMS particle, a parabolic profile is established.

## II.D. Bed Regeneration

### II.D.1. ZMS Variant

The model also aims to cover the regeneration of the bed. As the regeneration of the ZMS bed is also done by gas flow of a hot carrier gas, the same set of equations can be used with boundary conditions swapped to invert the flow direction (see Table I).

### II.D.2. NEG Variant

The NEG bed is regenerated by depressurizing and vacuum pumping with no external flow. Following the assumption of negligible intraparticle transport resistance, the regeneration of the NEG bed is governed by the effective pumping speed $S_{eff}$ in $m^3 \cdot s^{-1}$ of the auxiliary vacuum system. For the regeneration phase, the bed internals are assumed as a single volume element. Assuming no external leaks into the system, the pump-down equation for the getter bed at an installed getter mass $m_g$ is then

$$m_g \frac{dc}{dt} + V \frac{dp}{dt} = -pS_{eff} \ . \tag{10}$$

After the initial depressurizing, the amount of hydrogens absorbed far outweighs the gas contained in the volume, and hence, the $Vdp$ term can be neglected. Substituting Eq. (5) and integrating give an analytical solution for the concentration of hydrogen in the getter as

$$c(t) = \frac{1}{\frac{1}{c_0} + \frac{S_{eff}}{m_g K_S} t} \ , \tag{11}$$

which is used to calculate the required pumping speed for a given $c_0$ at the beginning and $c(t = \tau_C)$ at the end of the regeneration cycle.

We here assume isothermal regeneration for all cases reported of the NEG bed to avoid introducing additional thermal cycling fatigues on the pressure vessel

## III. RESULTS

To investigate the behavior of the bed, simulation cases are set up that represent a design point and operation conditions as per the DEMO preconceptual

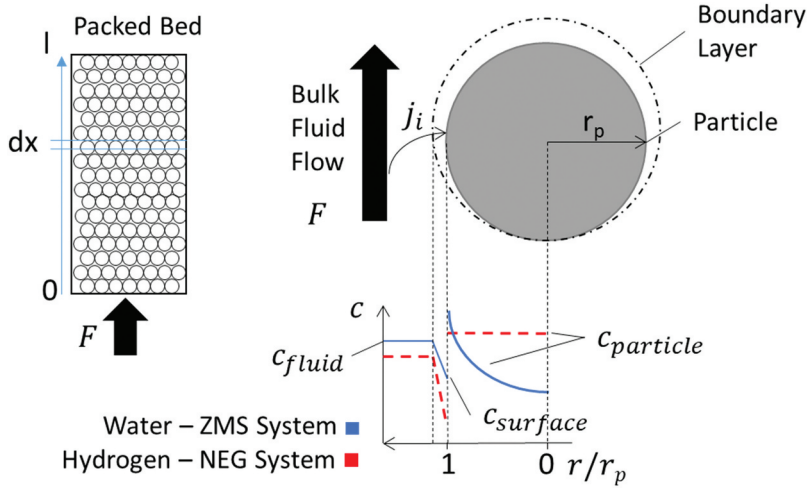


Fig. 3. Illustration of the transport behavior and concentration profiles in the packed bed, when considering boundary layer transport resistance only (NEG), as well as boundary and intraparticle transport resistance (ZMS). The value $j_i$ indicates the sorption flux from the bulk fluid phase to the particle.

design. For the ZMS variant, a water partial pressure of 1000.04 Pa is used (corresponding to the case of highest protium addition with complete conversion on CuO beds), whereas for the NEG variant, the case of 80 Pa of hydrogen is used. Both variants aim for a cycle time of $\tau_c$ = 4 days. As the initial condition of complete regeneration is not achievable under realistic process conditions (see Sec. III.B), the simulation is run for one full cycle before evaluations are performed. Table III then gives the configurations of the beds and feed stream employed in the simulation, and Table IV gives the thermophysical property data used.

TABLE III

Configuration for the Beds and Feed Stream Used in the Simulation, Based on the Preconceptual Design of the Process*

| | ZMS System | NEG System |
|---|---|---|
| $F_{feed}$ (mols$^{-1}$) | 750 | |
| $T_{feed}$(K) | 298 | 773 |
| $p_{feed}$(Pa) | $8 \times 10^6$ | |
| $d_b$(m) | 1.41 | 1.47 |
| $l_b$(m) | 3.0 | 3.7 |
| $d_p$(m) | 0.002 | |
| ε | 0.4 | |
| $m_s$(kg) | 3400 | 1050 |
| $\tau_c$(day) | 4 | |

*Reference 3.

TABLE IV

Thermophysical Property Data Used in the Simulations

| | |
|---|---|
| Helium viscosity, η (Pa·s) | 1.96e-5 ($T$ = 298 K)<br>3.12e-5 ($T$ = 573 K)<br>3.84e-5 ($T$ = 773 K) |
| Helium heat capacity, $c_{p,f}$ (J/mol·K$^{-1}$) | 20.1 |
| Water heat of adsorption on ZMS, $h_{ad}$ (J/mol·K$^{-1}$) | 54961 |
| ZMS heat capacity, $c_{p,s}$ (J/kg·K$^{-1}$) | 920 |
| ZMS surface heat transfer coefficient, α (W/m$^2$·K$^{-1}$) | 20 |

## III.A. Take-Up Phase

Figure 4 shows a time evolution of the sorption phase for the ZMS and NEG beds over time. Both systems are characterized by a concentration front that moves in flow direction with time [with the length of that front referred to as the mass transfer zone (MTZ) here]. For the ZMS system, the slope of this front is very sharp, occupying less than 8% of the total bed length, whereas the NEG variant exhibits a much broader MTZ, stretching 20% of the bed length. The difference may partially be explained by the shape of the respective isotherms (curves of sorbed amount versus partial pressure): For ZMS, the water isotherm is strong nonlinear, providing a large driving force gradient, even at high loading, whereas for NEG, the $H_2$ system diminishes proportional to its loading. The presence of this MTZ limits the usable bed capacity

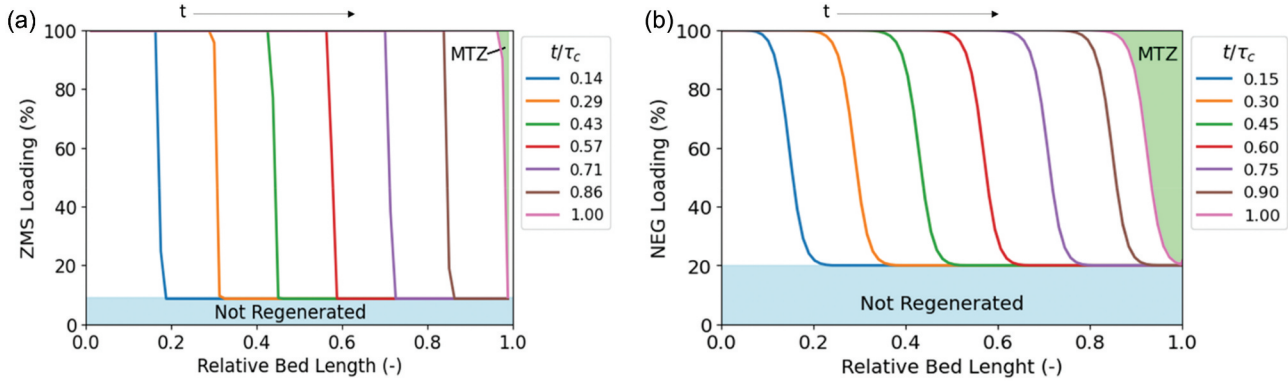


Fig. 4. Evolution of the sorption front with time for (a) the molecular sieve bed and (b) the getter bed. The green area indicates the amount of sorbent capacity that is unavailable due to the MTZ, and the blue area indicates the sorption capacity lost due to incomplete regeneration.

proportional to its size since the bed must be disconnected once the front of the MTZ reaches the bed outlet. A performance indicator is then the percentage of the unusable bed capacity due to this effect versus the theoretical installed total sorption capacity.

## III.B. Regeneration

### *III.B.1. ZMS Variant*

Once depressurized, regeneration of the ZMS bed is achieved by purging with a hot purge gas (assumed to also be helium here) in counterflow direction. The conditions of the purge gas stream are set as $F_{reg} = 10\,\mathrm{mol}\cdot\mathrm{s}^{-1}$, $p_{reg} = 1\times10^5\mathrm{Pa}$, $T_{reg} = 573.15\mathrm{K}$, with the flow rate selected to give a packed bed Reynolds number $\mathrm{Re}_b > 3$ to avoid the fully laminar flow regime. Figure 5a then shows the evolution of the loading front in the bed (solid lines), as well as the temperature distribution (dashed lines) for a bed previously saturated. As can be seen, the evolution of the loading front coincides with the temperature front, with the achievable regeneration rate consequently limited by the bed heating rate through the purge gas stream (no external heating is assumed here). In this scenario, the regeneration of the bed is nevertheless completed in less than 10% of the cycle time.

The total regeneration achievable is limited by the remaining water partial pressure after the condenser, with $p^*(T_{cond} = 275\mathrm{K}) = 700\mathrm{Pa}$. A corresponding remaining loading of 9.2% at the regeneration temperature is obtained from the equilibrium isotherm at the regeneration temperature (see Fig. 2b).

Figure 5b shows the flow rate of water extracted from the condenser for a sequence of three cycles. Because of the fast regeneration time, the flow rate peaks after the bed cycling at 106 $\mathrm{kg}\cdot\mathrm{h}^{-1}$, equaling an average steady-state flow rate of 6.1 $\mathrm{kg}\cdot\mathrm{h}^{-1}$ over the full cycle time.

### *III.B.2. NEG Variant*

The loading of the NEG during the regeneration process is shown in Fig. 6a for three different levels of effective auxiliary pumping speeds. As can be seen, the achievable regeneration within the cycle time is strongly dependent on the external pumping speed and exhibits an exponential behavior, resulting in diminishing returns toward lower loadings. The installed pumping speed is generally a trade-off between the achievable regeneration and the cost of the installed vacuum system. Targeting a regeneration to at least 80%, an effective pumping speed of at least 1 $\mathrm{m}^3\cdot\mathrm{s}^{-1}$ is required. The flow rate of the extracted stream then also shows the same exponential behavior. As is shown in Fig. 6b, after the initial

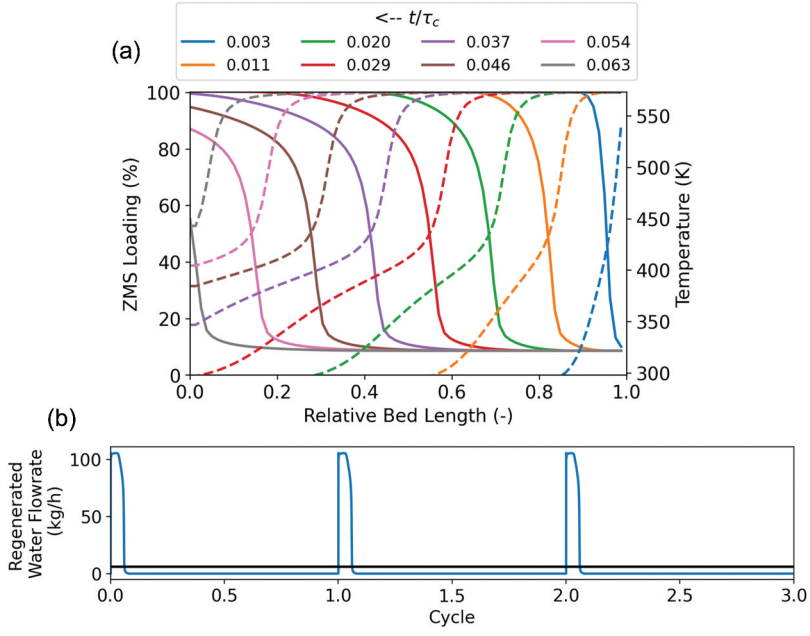


Fig. 5. (a) Evolution of the loading front in the ZMS bed in the regeneration phase. Solid lines refer to the ZMS loading in the left axis, and dashed lines indicate temperatures in the right axis. (b) Flow rate of liquid water extracted from the condenser in the regeneration loop after three cycles. The black lines indicate the time-averaged steady-state flow rate.

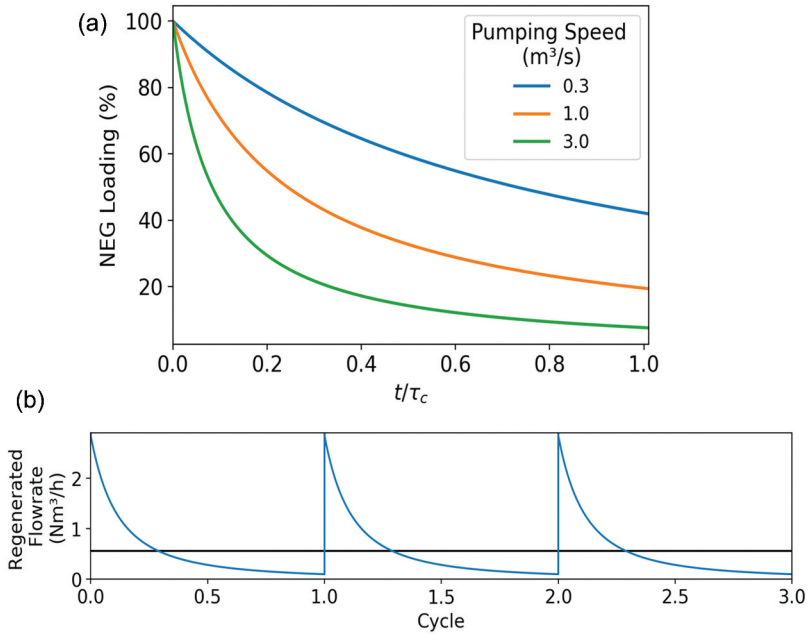


Fig. 6. (a) Regeneration loading of the NEG bed with time for three different levels of effective auxiliary pumping speed. (b) Flow rate of gas evacuated from the NEG bed for three cycles of the system when regenerating to at least 80%. The black lines indicate the time-averaged steady-state flow rate.

depressurization, the maximum flow rate peaks at 2.9 $Nm^3 \cdot h^{-1}$, with a time-averaged flow rate of 0.56 $Nm^3 \cdot h^{-1}$ over the full cycle time.

## IV. DISCUSSION

The above investigations allow calculation of the required sorbent masses to achieve a desired cycle time by factoring in the sorbent mass not utilized in each cycle due to the effects discussed above. The maximum capacity corresponds to the equilibrium loading everywhere in the bed, which is then diminished due to incomplete regeneration and the length of the MTZ that cannot be fully loaded.

Table V gives the values based on the results presented in Sec. III.

The required oversizing of the bed (or shortening of the cycle time) is offset by the achievable sorption efficiency of the bed (the actual amount of sorbate being captured), defined here as ratios of sorbate partial pressures at the inlet and outlet: $\eta_{CPS} = p_{s,in}/p_{s,out}$. The value $p_{s,out}$ can be evaluated by the achieved regeneration level and the equilibrium loading relationship of the respective variant [see Eqs. (5) and (6)] (in phases where the MTZ has not reached the end of the bed).

Figure 7 shows the achievable efficiency of the sorbents bed for both applications as a function of the achieved regeneration. Because of the strong nonlinearity of the molecular sieve isotherm, much higher efficiencies are achieved even at lower regeneration levels. The NEG variant in turn exhibits a nearly linear relationship. For the here achieved regenerations of 91% and 80%, $\eta_{CPS} > 99.9\%$ and $\eta_{CPS} = 93\%$ are achieved for the ZMS and NEG variants, respectively.

Because of the cyclic nature of the discharged streams, both require additional effort to integrate them into the fully continuous fuel cycle. The discharged water may be easily buffered by an appropriately sized tank, whereas the NEG variant requires the use of additional compressors and buffer vessels if one wants to create steady-state flow conditions.

TABLE V

Capacity Losses of the Sorbates on Account of the Size of the MTZ and Incomplete Regeneration

| | NEG, $p_{H2} = 80$Pa | ZMS, $P_{H2O} = 1000$Pa |
|---|---|---|
| Not regenerated | 20% | 9.2% |
| Mass transfer zone | 10% | 3.6% |
| Total | 30% | 12.8% |

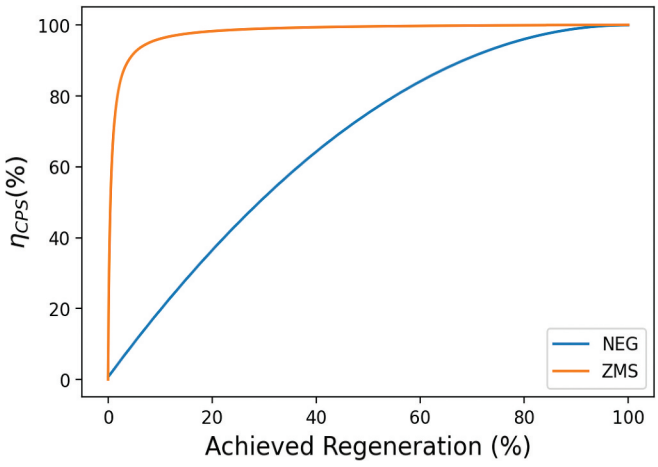


Fig. 7. Efficiencies of the sorbents bed as a function of the achieved regeneration of the bed capacity.

## V. CONCLUSIONS

The simulations clearly highlight one advantage of the ZMS process: achieving very high efficiencies of $\eta_{CPS} > 99.9\%$ with a well-proven technology available at a high technology readiness level. One concern however is the generation of liquid tritiated water. At protium additions below 130 Pa, activities upward of 500 Ci/kg are reached, which is considered undesirable from a safety perspective. The NEG process in turn avoids this conversion to water and offers a simpler system layout but is limited to hydrogen partial pressure below 300 Pa at the given coolant temperatures, as to not encounter fast material degradation due to embrittlement. Even if the performance estimated for the NEG solution of $\eta_{CPS} = 93\%$ is lower than the ZMS process, it is still above the required limit of 90%.

Given the uncertainty in the $H_2$ content in helium primary coolant, we can conclude that the ZMS process is the preferable option for the case in which the $H_2$ addition is greater than 300 Pa while for lower $H_2$ values, the NEG option is preferable due to process simplicity and because it avoids production of tritiated water that then needs further processing. Once a reference scenario has been identified, the numerical implementation of the developed model can be used to support the sizing of the sorption bed for both variants as well as predict the systems output toward downstream processing operations tasked with tritium recovery.

In order to mature the technology readiness level of the NEG variant, thorough experimental characterization of the NEG material in DEMO-relevant application is foreseen whereas the ZMS process can benefit heavily from return of experience in the ITER TBM program.

## Disclaimer

Views and opinions expressed are however those of the author(s) only and do not necessarily reflect those of the European Union or the European Commission. Neither the European Union nor the European Commission can be held responsible for them.

## Disclosure Statement

No potential conflict of interest was reported by the authors.

## Funding

This work has been carried out within the framework of the EUROfusion Consortium, funded by the European Union via the Euratom Research and Training Programme [Grant Agreement No. 101052200 — EUROfusion].

## ORCID

Jonas C. Schwenzer http://orcid.org/0000-0001-6064-4332

## References

1. G. A. SPAGNUOLO et al., "Integrated Design of Breeding Blanket and Ancillary Systems Related to the Use of Helium or Water as a Coolant and Impact on the Overall Plant Design," *Fusion Eng. Des.*, **173**, 112933 (2021); https://doi.org/10.1016/j.fusengdes.2021.112933.
2. F. FRANZA et al., "Tritium Permeation Issued for Helium-Cooled Breeding Blankets" *Proc. 2013 IEEE 25th*

*Symp. Fusion Engineering (SOFE*), San Francisco, California, June 10–14, 2013, p. 1, IEEE (2013), https://doi.org/10.1109/SOFE.2013.6635335.

3. A. SANTUCCI et al., "The Issue of Tritium in DEMO Coolant and Mitigation Strategies," *Fusion Eng. Des.*, **158**, 111759 (2020); https://doi.org/10.1016/j.fusengdes.2020.111759.

4. C. DAY et al., "The Pre-Conceptual Design of the DEMO Tritium, Matter Injection and Vacuum Systems," *Fusion Eng. Des.*, **179**, 113139 (2022); https://doi.org/10.1016/j.fusengdes.2022.113139.

5. I. RICAPITO et al., "Tritium Processing Systems for the Helium Cooled Pebble Bed Test Blanket Module," *Fusion Eng. Des.*, **83**, *10–12*, 1461 (2008); https://doi.org/10.1016/j.fusengdes.2008.05.041.

6. F. SIVIERO et al., "Characterization of ZAO® Sintered Getter Material for Use in Fusion Applications," *Fusion Eng. Des.*, **146**, *Part B*, 1729 (2019); https://doi.org/10.1016/j.fusengdes.2019.03.026.

7. A. SANTUCCI et al., "Novel Non-Evaporable Getter Materials and Their Possible Use in Fusion Application for Tritium Recovery," *Molecules*, **25**, 5675 (2020); https://doi.org/10.3390/molecules25235675.

8. S. ERGUN and A. A. ORNING, "Fluid Flow Through Randomly Packed Columns and Fluidized Beds," *Ind. Eng. Chem.*, **41**, 1179 (1949); https://doi.org/10.1021/ie50474a011.

9. A. SIEVERTS, "The Absorption of Gases by Metals," *Z. Met*., **21**, 37 (1929).

10. Y. WANG, "Measurements and Modeling of Water Adsorption Isotherms of Zeolite Linde-Type A Crystals," *Ind. Eng. Chem. Res.*, **59**, 8304 (2020); https://doi.org/10.1021/acs.iecr.9b06891.

11. N. WAKAO and T. FUNAZKRI, "Effect of Fluid Dispersion Coefficients on Particle-to-Fluid Mass Transfer Coefficients in Packed Beds: Correlation of Sherwood Numbers," *Chem. Eng. Sci.*, **33**, 1375 (1978); https://doi.org/10.1016/0009-2509(78)85120-3.

12. E. GLUECKAUF, "Theory of Chromatography. Part 10.—Formulae for Diffusion into Spheres and Their Application to Chromatography," *Trans. Faraday Soc*., **51**, 1540 (1955); https://doi.org/10.1039/TF9555101540.

13. J. KÄRGER and D. RUTHVEN, *Diffusion in Zeolites and Other Microporous Solids*, Wiley & Sons, New York (1992).

14. E. FULLER et al., "Diffusion of Halogenated Hydrocarbons in Helium. The Effect of Structure on Collision Cross Sections," *J. Phys. Chem.*, **73**, 367 (1969); https://doi.org/10.1021/j100845a020.